A MEMS-BASED SPIRAL PIEZOELECTRIC ENERGY HARVESTER

Tao Dong[1], Einar Halvorsen[1], Zhaochu Yang[2]
[1] Institute for Microsystem Technology, R. I. , Vestfold University College, Tønsberg, Norway
[2] State Key Lab of Multiphase Flow in Power Engineering, Xi'an Jiaotong University, Xi'an, China

Abstract: A spiral piezoelectric energy harvester (SPEH) suited for micro-fabrication and sensitive to in-plane vibrations is proposed in this paper. A mode 31 coupling is realized with the electrode configuration functioning for both poling and transduction. With the moment caused by large proof mass considered, the intrinsic characteristics of the SPEH were explored by FEM simulations. Then the output power is evaluated at several tens of micro-watts with an acceleration of 5g by use of a simplified analytical model. It is found the output power depends on frequency and direction of the external force as well as the resistance load.

Key words: spiral piezoelectric energy harvester (SPEH), MEMS, model, vibration, in-plane

1. INTRODUCTION

Scavenging energy from environmental vibrations calls for devices working with low resonant frequency [1]. The spiral piezoelectric energy harvester (SPEH) presents a promising solution since the tangential displacement at the tip of a spiral is several times that of an equivalent length straight ceramic strip [2]. Numerical study on the electromechanical behavior of the spiral-shaped actuator was reported by Chen et al. [3]. A spiral cantilever was designed to achieve compactness, low resonant frequency and minimum damping coefficient by Choi et al. [4]. However, when the spiral cantilever vibrates out of plane, the stress varies alternately from stretching to compressing along the cantilever, which leads to insuppressible difficulty in designing a feasible electrode configuration. A piezoelectric spiral-belt bimorph in coupled flexural-extensional modes for scavenging ambient vibration energy was analyzed by Hu et al. [5]. Their work focused on theoretical discussion based on the availability of ceramic spiral actuators.

In this work, a MEMS-based SPEH is proposed with a coupling mode 31. The basic properties of the SPEH such as the stiffness matrix and electromechanical parameters are obtained by finite element analysis. These are then used as input to a simple analytical model. Due to the large dimensions of the proof mass considered, the resulting moment acting on the spring end can not be neglected, but is accounted for in the analytical model. The output power is evaluated at a given external vibration amplitude and frequency.

2. STRUCTURE DESIGN

The schematic of the SPEH is shown in Fig.1, which consists of two independent Archimedes' spiral springs, sharing the same anchor in the center of the device within an area of 13mmX13mm. Each of the spiral cantilevers large proof mass (425 μm thick) mounted beneath the free end having the arc length of a quarter circle (Fig.1b); therefore, the natural frequency was effectively reduced to match the environmental vibrations. With sufficient out of plane (z-axis) stiffness, the SPEH will only vibrate in-plane. In a practical device, top and bottom wafers will further constrain motion in the thickness direction under extreme conditions.

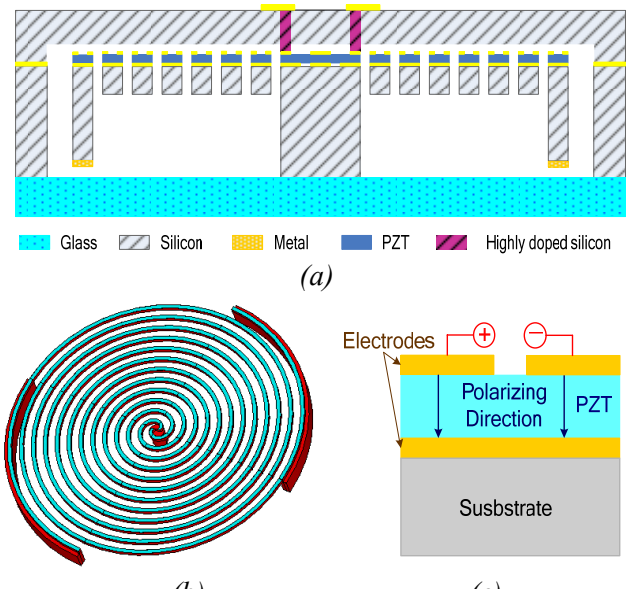

Fig. 1: Schematic structure of the SPEH working in-plane: (a) side view; (b) perspective drawing; electrode configuration.

The electrode configuration of the SPEH is shown in Fig. 1c. The PZT film is polarized in the thickness direction. The electrodes on the top surface of the spiral cantilever are split along the length direction realizing a d_{31} coupling.

Modal analysis of the SPEH was performed to determine the resonant frequencies and vibration modes. The dimensions of the spiral cantilever and the proof mass were adjusted to yield in-plane working modes. The finally determined spiral spring has a cross-section of 150μmX150μm. The lowest 3 natural frequencies were evaluated at 62.6Hz, 184.4Hz, and 262.6Hz. The corresponding vibration modes are illustrated in Fig. 2, and are all purely in-plane.

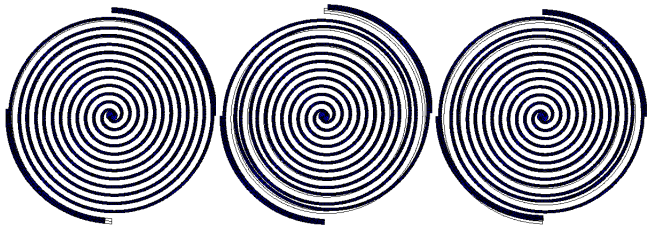

(a) (b) (c)

Fig. 2: The 1-3 modes of the SPEH vibration in-plane.

3. MODELING

Assuming there is small deformation within elastic range for the spiral cantilever the electromechanical coupling characteristics of the SPEH can be described by,

$$\boldsymbol{F}_{\mathrm{l}} = \boldsymbol{K}_{\mathrm{sc}}\boldsymbol{U}_{\mathrm{l}} - \boldsymbol{\Gamma}V\,, \tag{1}$$

$$q = \boldsymbol{\Gamma}^{\mathrm{T}}\boldsymbol{U}_{\mathrm{l}} + C_{\mathrm{CL}}V\,. \tag{2}$$

in which $\boldsymbol{K}_{\mathbf{sc}}$ is the short circuit stiffness matrix with components

$$\boldsymbol{K}_{\mathrm{sc}} = \begin{bmatrix} k_{\mathrm{y}} & k_{\mathrm{y}\theta} & k_{\mathrm{yx}} \\ k_{\theta\mathrm{y}} & k_{\theta} & k_{\theta\mathrm{x}} \\ k_{\mathrm{xy}} & k_{\mathrm{x}\theta} & k_{\mathrm{x}} \end{bmatrix} \tag{3a}$$

$\boldsymbol{\Gamma}$, the vector of coupling factors

$$\boldsymbol{\Gamma} = \begin{bmatrix} \gamma_{\mathrm{y}} & \gamma_{\theta} & \gamma_{\mathrm{x}} \end{bmatrix}^{\mathrm{T}} \tag{3b}$$

and C_{CL}, the clamped capacitance.

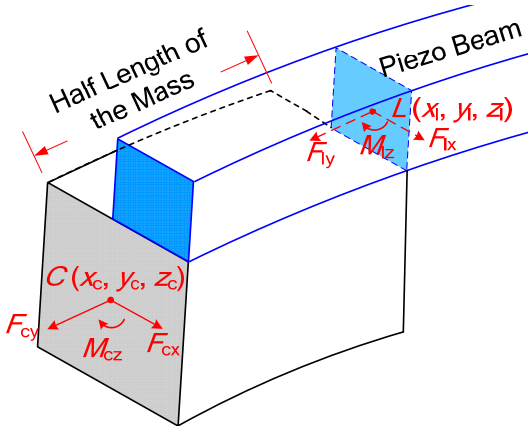

Fig. 3: Schematic of the spiral beam connected with the large proof mass.

Due to the large dimensions of the proof mass, it is not reasonable to treat it as a concentrated mass. That is, the moment on the beam caused by the large proof mass has to be taken into account. Consider the proof mass of the SPEH (Fig. 3), the motion in-plane has 3 mechanical degrees of freedom (DOF), i.e. $\boldsymbol{U}_c = [y_c,\ \theta_c,\ x_c]$. The equations of motion for the large mass is,

$$\boldsymbol{M}\ddot{\boldsymbol{U}}_{\mathrm{c}} = -\tilde{\boldsymbol{K}}_{\mathrm{sc}}\boldsymbol{U}_{\mathrm{c}} - \alpha\boldsymbol{M}\dot{\boldsymbol{U}}_{\mathrm{c}} + \tilde{\boldsymbol{\Gamma}}V + \boldsymbol{F}_{\mathrm{ext}} \tag{4}$$

where $\boldsymbol{F}_{\mathrm{ext}}$=[m$a_y$ *0* ma_x] is the external (fictitious) force. Equation (2) can be written as,

$$q = \tilde{\boldsymbol{\Gamma}}^{\mathrm{T}}\boldsymbol{U}_{\mathrm{c}} + C_{\mathrm{CL}}V \tag{5}$$

$$\boldsymbol{U}_{\mathrm{l}} = \boldsymbol{T}\cdot\boldsymbol{U}_{\mathrm{c}}\,,\ \boldsymbol{F}_{\mathrm{l}} = \left(\boldsymbol{T}^{\mathrm{T}}\right)^{-1}\cdot\boldsymbol{U}_{\mathrm{c}} \tag{6a}$$

$$\tilde{\boldsymbol{\Gamma}} = \boldsymbol{T}^{\mathrm{T}}\boldsymbol{\Gamma}\,,\ \tilde{\boldsymbol{K}}_{\mathrm{sc}} = \boldsymbol{T}^{\mathrm{T}}\boldsymbol{K}_{\mathrm{sc}}\boldsymbol{T} \tag{6b}$$

where T is the matrix

$$\boldsymbol{T} = \begin{bmatrix} 1 & -|y_{\mathrm{l}} - y_{\mathrm{c}}| & 0 \\ 0 & 1 & 0 \\ 0 & -|x_{\mathrm{l}} - x_{\mathrm{c}}| & 1 \end{bmatrix} = \begin{bmatrix} 1 & -2.0045\text{e-}3\mathrm{m} & 0 \\ 0 & 1 & 0 \\ 0 & -3.8073\text{e-}3\mathrm{m} & 1 \end{bmatrix} \tag{7}$$

Assuming a purely resistive load with resistance R, the electrical equation is simply Ohms law

$$V = -R\dot{q} \tag{8}$$

Substituting equation (5) in equation (8), we get

$$V = -R\left(\tilde{\boldsymbol{\Gamma}}^{\mathrm{T}}\dot{\boldsymbol{U}}_{\mathrm{c}} + C_{\mathrm{CL}}\dot{V}\right) \tag{9}$$

Now set

$$\boldsymbol{U}_{\mathrm{c}} = \mathrm{R}_{\mathrm{e}}\left\{\hat{\boldsymbol{U}}_{\mathrm{c}}e^{i\omega t}\right\}, \tag{10a}$$

$$V = \mathrm{R}_{\mathrm{e}}\left\{\hat{V}e^{i\omega t}\right\}, \tag{10b}$$

$$\boldsymbol{F}_{\mathrm{ext}} = \mathrm{R}_{\mathrm{e}}\left\{\hat{\boldsymbol{F}}_{\mathrm{ext}}e^{i\omega t}\right\}, \tag{10c}$$

equation (4) and equation (9) can be rewritten as,

$$-\omega^2\boldsymbol{M}\hat{\boldsymbol{U}}_{\mathrm{c}} = -\tilde{\boldsymbol{K}}_{\mathrm{sc}}\hat{\boldsymbol{U}}_{\mathrm{c}} - \alpha\boldsymbol{M}\cdot i\omega\cdot\hat{\boldsymbol{U}}_{\mathrm{c}} + \tilde{\boldsymbol{\Gamma}}\hat{V} + \hat{\boldsymbol{F}}_{\mathrm{ext}} \tag{11}$$

$$\hat{V} = -R\left(\tilde{\boldsymbol{\Gamma}}^{\mathrm{T}}\cdot i\omega\cdot\hat{\boldsymbol{U}}_{\mathrm{c}} + C_{\mathrm{CL}}\cdot i\omega\cdot\hat{V}\right) \tag{12}$$

where we set α=23.274 to get a quality factor Q=50; $\omega = 2\pi f$ for the second mode, see Fig. 2b. From (11) and (12), by eliminating the vector $\tilde{U}_c$, we get

$$\hat{V} = \frac{-i\omega R}{1 + i\omega C_{\mathrm{CL}}R}\cdot\tilde{\boldsymbol{\Gamma}}^{\mathrm{T}} \cdot\left[\tilde{\boldsymbol{K}}_{\mathrm{sc}} - \omega^2\boldsymbol{M} + i\omega\alpha\boldsymbol{M} + \frac{i\omega R}{1 + i\omega C_{\mathrm{CL}}R}\tilde{\boldsymbol{\Gamma}}\cdot\tilde{\boldsymbol{\Gamma}}^{\mathrm{T}}\right]^{-1}\cdot\hat{\boldsymbol{F}}_{\mathrm{ext}} \tag{13}$$

which relates the output voltage to the external force directly. Therefore, the output power of the SPEH can be evaluated by,

$$P_{\mathrm{out}} = \left|\hat{V}\right|^2 \Big/ \left(2R\right) \tag{14}$$

It should be noticed that equation (13) and (14) are based on the assumption that there is no contact between the two spiral cantilevers. If contact occurs,

the validity of equation (14) is at best questionable. To avoid contact, the maximum displacement of the spiral cantilever should not exceed the distance between the two cantilevers. Moreover, the maximum rotation angle should be within a certain range. That is,

$$|\boldsymbol{U}_c| \le L_{gap} \quad \text{and} \quad \theta \le \theta_{max} \qquad (15)$$

in which L_{gap} is the geometric distance between the two spiral cantilevers; and θ_{max} is the maximum angle that could be accepted as small deformation. In this work, L_{gap}= 400μm, and θ_{max} =0.077 rad by using; for the latter, simple error criteria on the trigonometric identities to have at most 0.1% error.

4. RESULTS AND DISCUSSION

4.1 Intrinsic parameters and vibration modes

PZT4D was used as the piezoelectric material having thickness of 2μm in the SPEH. The intrinsic parameters of the SPEH, those involved in equation (1) and (2), are determined by FEA simulation, as listed in Table 1.

Table 1: Intrinsic parameters of the SPEH

Parameters	Value	Parameter	Value
k_x (N/m)	7.9360	γ_x (N/V)	-0.2312e-6
k_y (N/m)	7.5575	γ_y (N/V)	-0.2327e-5
k_θ (Nm/Rad)	0.3141e-3	γ_θ (Nm/V)	-0.1619e-7
k_{xy} (N/m)	-0.4016		
$k_{x\theta}$ (N/Rad)	-0.4657e-2	C_{CL} (pF)	2714.5
$k_{y\theta}$ (N/Rad)	-0.4344e-1		

* Due to the symmetry of the stiffness matrix, it has $k_{yx}= k_{xy}$, $k_{\theta x}= k_{x\theta}$, $k_{y\theta}= k_{\theta y}$.

4.2 Static analysis

The static analysis for the SPEH was performed to reveal mechanical characteristics while a constant acceleration of 5g was added in either x- or y-direction. The typical distributions of the stress under different acceleration directions are illustrated in Fig. 4. It is found that the stresses in tangent and radial direction are considerable while the shear stress in-plane is quite low and can be neglected in this structure.

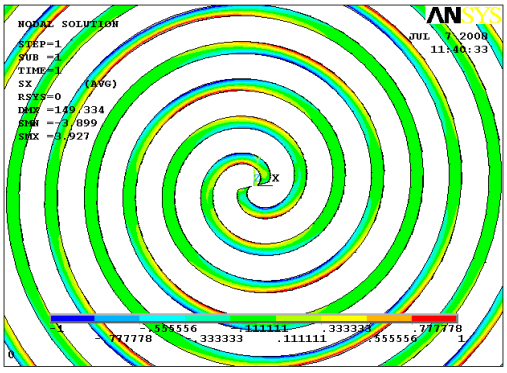

(a)

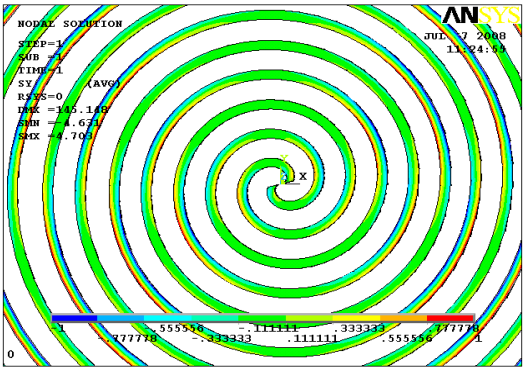

(b)

Fig. 4: The typical stress distribution in the PZT film, (a) x-component of normal stress for acceleration in x-direction; (b) y-component of normal stress for acceleration in x-direction.

Fig. 5 illustrates the electric field distribution in the middle plane of PZT film. It shows that the electric potential between the inner and out sides of spiral cantilever is quite regular. This indicates a reasonable agreement with the electrode configuration shown in fig.1c.

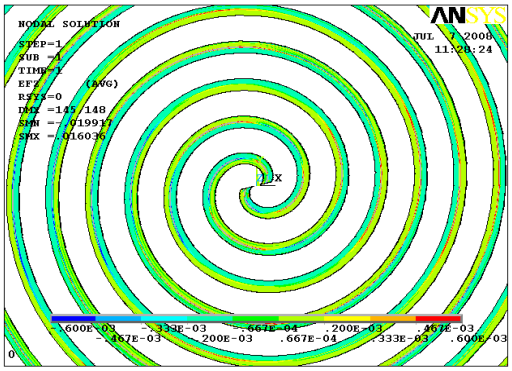

Fig. 5: Open circuit electric field in the middle plane of PZT film with 5g acceleration in x-direction.

4.3 Output power

According to the model described in section 3, the output performance of the SPEH was evaluated by Matlab. Acceleration with the amplitude value of 5g was added to the SPEH. Several directions of the acceleration were checked and the results were listed in Table 2.

Table 2: Output power vs. direction of the force

Direction	Max. power	Displacement
rad	μW	μm
0	19.72	34.7
π/4	25.12	94.2
π/2	22.69	68.5
3π/4(*)	4.90	191.2
π	19.72	34.7
5π/4	25.12	94.2
3π/2	22.69	68.5
7π/4(*)	4.90	191.2

(*) *represents the maximum power occurs at the third natural frequency.*

It can be noticed that the output power of the SPEH is rather considerable. All the displacements corresponding to the maximum power are within the allowable range and the maximum rotation angle is checked not beyond 0.0025rad, far below the value of θ_{max}. Fig. 6 plots a typical output power varying with the external frequency with resistance load 630kΩ, $\phi=\pi/2$. There are 3 peaks of power in the case, corresponding to the three natural frequencies. However, the maximum value appears not at the first natural frequency but the second one. This is in agreement with the analytical results reported by Hu et al. [5]. It can also read the eigenfrequencies from Fig.6, namely, 62.5Hz, 183.6Hz, and 260.2Hz, which are quite close to those obtained by FEA.

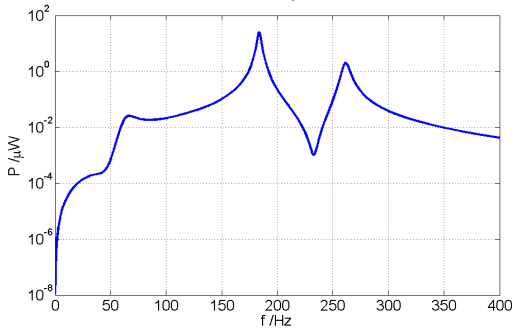

Fig. 6: The output power of the SPEH under acceleration with the amplitude of 5g, and load resistance 630kΩ.

In Fig. 7a and b, the output performance of the SPEH is shown as it varies with load resistance and direction of external force respectively when the excitation frequency ranges from 1Hz to 400 Hz. The output power depends heavily on load resistance, direction of the acceleration and vibration frequency. We find that when the direction is $\phi=\pi/4$ or $\phi=5\pi/4$, the output power has an extremum at 25.12μW.

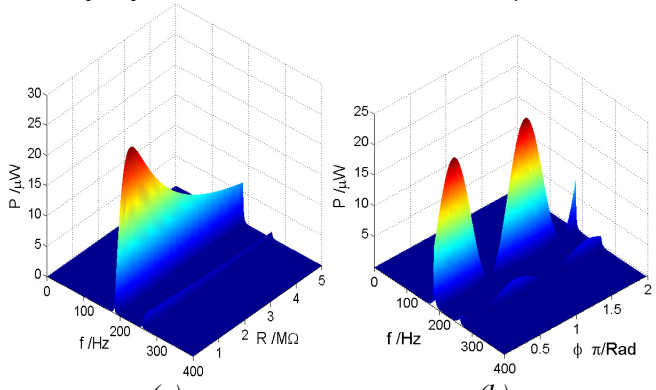

(a) *(b)*

Fig. 7: The output power of the SPEH versus (a) resistance load with $\phi=\pi/2$; (b) the direction of external acceleration with R=630kΩ.

5. CONCLUSIONS

A MEMS-based SPEH working in-plane for ambient scavenging vibration energy is proposed and analyzed in this work. Two spiral cantilevers mechanically independent but electrically connected in series give a compact design within an area of 13mmX13mm. The electrode configuration is designed and a mode 31 coupling is realized. With the moment caused by the large dimensions of the proof mass considered, an analytical model was developed to evaluate the output power when suffering random external acceleration. The intrinsic characteristics of the SPEH are explored by FEA simulation.

The results show that the output power depends on not only the external frequency but also the direction of the external acceleration and resistance load. A maximum power 25.12 μW is found at the second natural frequency and a resistance load 630kΩ. This means the SPEH proposed in this work could be feasible for powering portable electric devices.

ACKNOWLEDGEMENT

This research work is supported by Natural Science Foundation of Fujian Province, China (No.2007J0032), National Natural Science Foundation of China (No.50406019) and Norwegian regional government funds (project BTV-Teknologi).

REFERENCES

[1] Sodano H A. and Inman D J 2004 A review of power harvesting from vibration using piezoelectric materials *The Shock and Vibration Digest* **36** 197-205

[2] Mohammadi F, Kholkin A L, Jadidian B, Safari A 1999 High-displacement spiral piezoelectric actuators *Appl Phys. Lett.* **75** 2488-2490

[3] Chen B, Sheeseman B A, Safari A, Danforth S C, Chou T W 2002 Theoretical and numerical predictions of the electromechanical behavior of spiral-shaped lead zirconate titanate (PZT) actuators. *IEEE Trans. Ultrasonics, Ferroelectrics, and Frequency Control* 49 319-326.

[4] Choi W J, Jeon Y., Jeong J H, Sood R, Kim S G 2006 Energy harvesting MEMS device based on thin film piezoelectric cantilevers. *J. Electroceram.* **17** 543-548

[5] Hu Y, Hu H, and Yang J 2006 A low frequency piezoelectric power harvester using a spiral-shaped bimorph. *Science in China Series G: Physics, Mechanics & Astronomy* **49** 649-659